"Chemical-substitution-driven giant anomalous Hall and Nernst effects in magnetic cubic Heusler compounds"

Guangzong Xing,[1,*] Keisuke Masuda,[1,2,†] Terumasa Tadano,[1,2] and Yoshio Miura[1,2]

[1] *Research Center for Magnetic and Spintronic Materials, National Institute for Materials Science, Tsukuba, Ibaraki, 305-0047, Japan*

[2] *Digital Transformation Initiative Center for Magnetic Materials, National Institute for Materials Science, Tsukuba, Ibaraki, 305-0047, Japan*

A. Comparison of the band structure

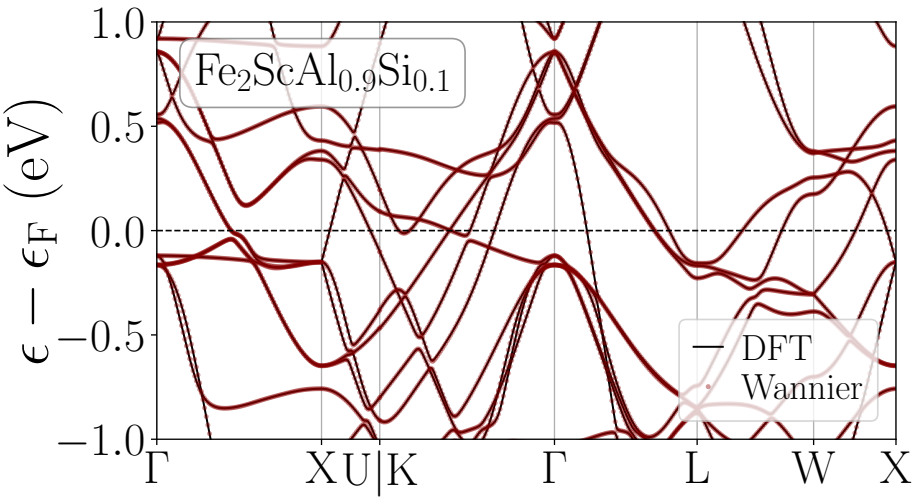

Figure S1. Comparison of the band structure of $Fe_2ScAl_{0.9}Si_{0.1}$ obtained based from DFT calculation (black curves) and Wannierization (red dots), respectively.

B. Detailed parameters of Wannierization

In this study, we generate the Wannier functions using the selected columns of the density matrix (SCDM) method. Two pivotal parameters, namely μ_{SCDM} and σ_{SCDM} are automatically

* XING.Guangzong@nims.go.jp
† MASUDA.Keisuke@nims.go.jp

determined through our developed Python scheme. Since the bands are entangled, we exclude 24 semi-core states and proceed to extract the target Wannier functions from twice as many Bloch states. In the disentangle procedure, two energy windows (outer and inner) are applied. We have found that choosing the appropriate outer window is crucial to obtaining accurate Wannier functions. The initial lower (upper) bound $\epsilon_{\max}$ ($\epsilon_{\min}$) of the outer window is chosen to be the lowest (highest) eigenvalue of the target states. In addition, the inner window is fixed to be $[\epsilon_{\min} : \epsilon_{\mathrm{F}} + 5]$ eV, where ϵ_{F} represents the Fermi energy. Subsequently, the energy difference denoted as $\Delta\epsilon$ (as detailed in the main text) is evaluated. If $\Delta\epsilon > 2$ meV, the Wannierization will be repeated with an increase in the upper bound of the outer window with a step of 2 eV. Ultimately, it is worth noting that ∼98% of the investigated candidates meet the predefined criterion.

C. Anomalous transport properties associated with the space group

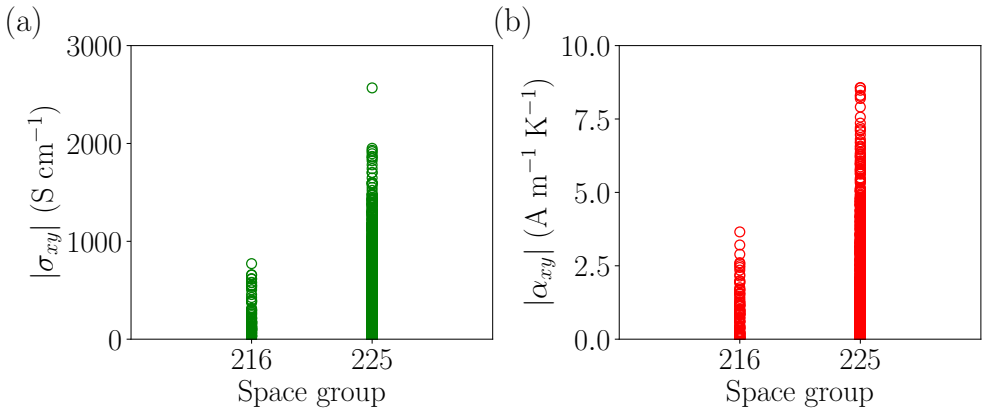

Figure S2. Calculated absolute values of anomalous Hall conductivity σ_{xy} (a) and anomalous Nernst conductivity α_{xy} (b) for regular (space group $Fm\bar{3}m$ # 225) and inverse (space group $F\bar{4}3m$ # 216) Heusler compounds.

D. Validity of the band-filling approach

To quantify the difference between the band-filling and the virtual crystal approximation (VCA) approaches, we introduced two metrics, $\Delta I_{T_{xy}}$ and $I_{T_{xy}}$. They are defined as follows:

$$\Delta I_{T_xy} = \int_{-0.1}^{0.1} \left| T_{xy}^{\mathrm{stoichio}}(\epsilon + \delta) - T_{xy}^{\mathrm{substi}}(\epsilon) \right| d\epsilon \tag{S1}$$

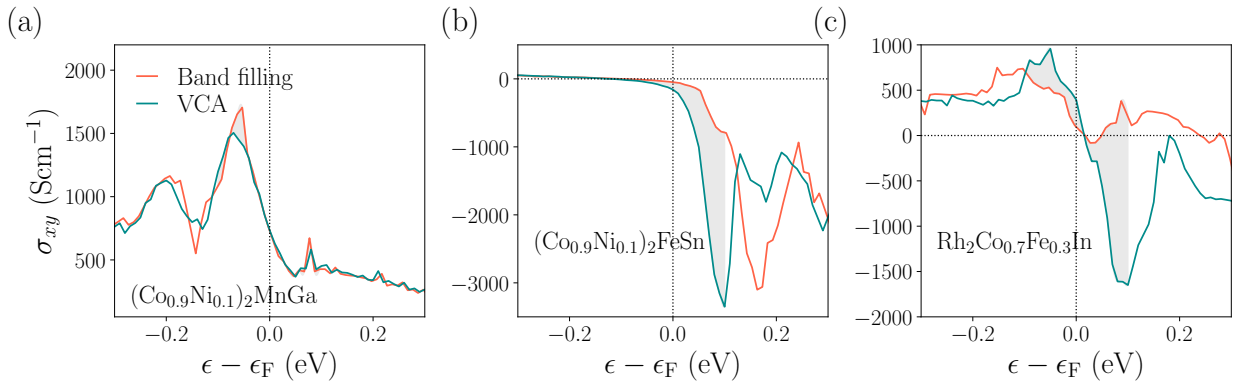

Figure S3. Comparison of energy-dependent σ_{xy} for $(Co_{0.9}Ni_{0.1})_2MnGa$ (a) and $(Co_{0.9}Ni_{0.1})_2FeSn$ (b), and $Rh_2Co_{0.7}Fe_{0.3}In$ (c), obtained based on the VCA and band-filling approach, respectively.

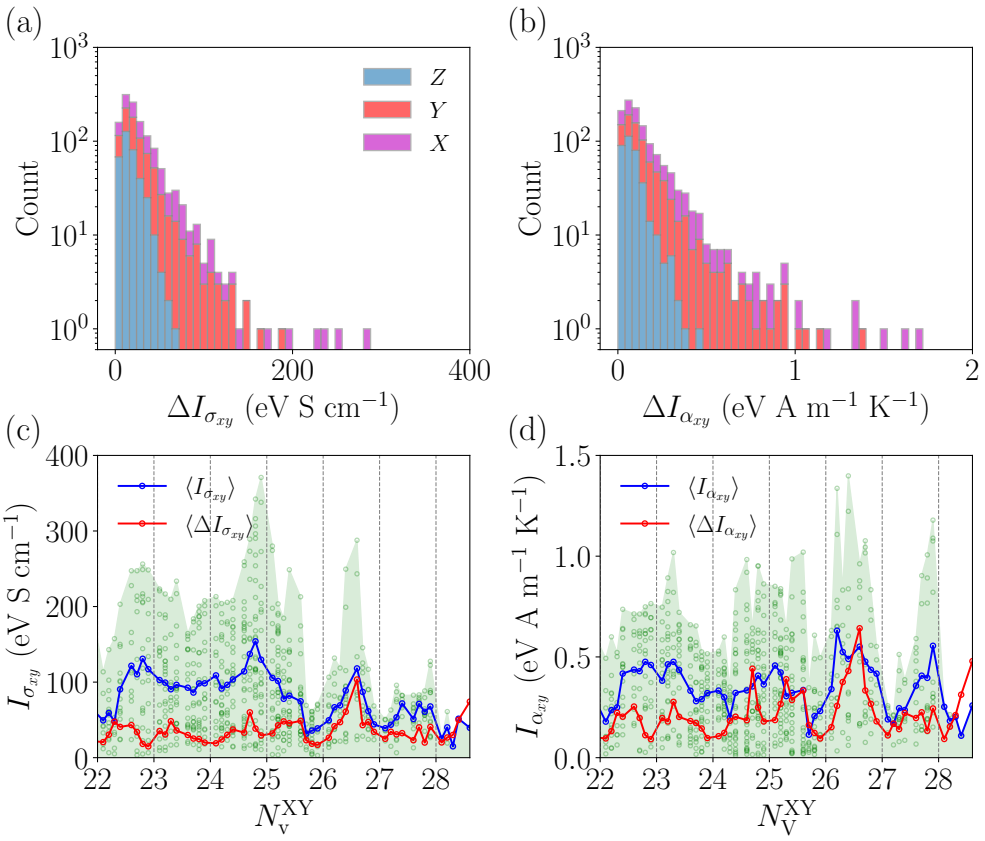

Figure S4. Histogram of $\Delta I_{\sigma_{xy}}$ (a) $\Delta I_{\alpha_{xy}}$ (b) with chemical substitution at X, Y, and Z sites, respectively. Calculated $I_{\sigma_{xy}}$ (c) and $I_{\alpha_{xy}}$ (d) with respect to the number of valence electrons at Y and Y sites N_v^{XY}. The red and blue lines show the average values of $\Delta I_{T_{xy}}$ and $I_{T_{xy}}$ (see text).

$$I_{T_{xy}} = \int_{-0.1}^{0.1} \left| T_{xy}^{\text{substi}}(\epsilon) \right| d\epsilon \tag{S2}$$

where $\Delta I_{T_{xy}}$ quantifies the discrepancy in the energy-dependent curves of transport quantities (refer to the gray area shown in Fig. S3 for σ_{xy}), with T_{xy} representing σ_{xy} or α_{xy}, between the VCA and band-filling approaches within and energy range of [−0.1:0.1] eV around the Fermi energy. $I_{T_{xy}}$ represents the integrated magnitude of the transport quantities around the Fermi energy. The energy shift δ, due to chemical substitution, is determined within the stoichiometric compounds using the band-filling approach.

As shown in Fig. S4(a) and (b), the $\Delta I_{\sigma_{xy}}$ and $\Delta I_{\alpha_{xy}}$ values tend to be small when the substitution occurs at the Z site, to which the band-filling approach potentially remains applicable. By contrast, a substitution at the X or Y site tends to give larger $\Delta I_{\sigma_{xy}}$ and $\Delta I_{\alpha_{xy}}$ values. This is expected because the density of states for p states near the Fermi energy from the Z site is much smaller than that for d states from the X and Y sites.

In the following, we focus on the cases where a substitution occurs either at the X or Y site and show how $\Delta I_{\sigma_{xy}}$ and $\Delta I_{\alpha_{xy}}$ behave with the total number of valence electrons at these sites, N_{v}^{XY}. Figures S4(c) and (d) present the scatter plots of the $I_{\sigma_{xy}}$ and $I_{\alpha_{xy}}$ (green circles), and the average values of $I_{T_{xy}}$ (blue circles) and $\Delta I_{T_{xy}}$ (red circles) as a function of N_{v}^{XY}. Here, we have excluded candidates with $N_{\mathrm{v}}^{XY} \leq 22$, as the values of σ_{xy} and α_{xy} are small in that region. The non-zero values of $\langle \Delta I_{T_{xy}} \rangle$ for all candidates, which are observed across all N_{v}^{XY}, clearly highlight the discrepancies in the anomalous transport quantities predicted by the band-filling and the VCA approaches. In particular, the highest values of $\langle \Delta I_{T_{xy}} \rangle$ were observed at $N_{\mathrm{v}}^{XY} \sim 26.5$, as shown in Figs. S4(c) and (d), indicating complete failure of the band-filling approach in this region. Moreover, unlike the singular peak value of $\langle \Delta I_{\sigma_{xy}} \rangle$, at $N_{\mathrm{v}}^{XY} \sim 26.5$, multiple peak values of $\langle \Delta I_{\alpha_{xy}} \rangle$ were observed (refer to Fig. S4(d) for $N_{\mathrm{v}}^{XY} \in [24{:}27]$), making the band-filling approach hardly justifiable for predicting α_{xy}.

The non-zero values of $\langle \Delta I_{T_{xy}} \rangle$ alone already demonstrate the limitations of the band-filling approach. However, since our study primarily targets chemically substituted candidates exhibiting significant anomalous transport quantities, the $\langle I_{T_{xy}} \rangle$ values are also relevant. As shown in Figs. S4(c) and (d), notable $\langle I_{T_{xy}} \rangle$ were observed with N_{v}^{XY} values around 23, 25 and 26.5. This observation suggests a strategic emphasis on the candidates with these N_{v}^{XY} values to achieve substantial σ_{xy} and α_{xy} values. Particularly noteworthy are the simultaneously large $\langle I_{T_{xy}} \rangle$ and $\langle \Delta I_{T_{xy}} \rangle$ with N_{v}^{XY} around 26.5, indicating promising candidates not predictable by the band-filling approach. For example, the VCA predicts significant σ_{xy} values for $(\mathrm{Co}_{0.8}\mathrm{Ni}_{0.2})_2\mathrm{Fe}Z$ (Z = Sn, Ge)

at $N_{\mathrm{v}}^{XY} = 26.4$—values unattainable via the band-filling approach. This discrepancy further underscores the VCA's importance in accurately calculating anomalous transport properties.

E. Anomalous transport properties in Fe- and Co-based Heusler alloys

As emphasized in the main text the substantial α_{xy} shown in Fig. S6(d) can be distinctly attributed to two significant Berry curvatures (BC) depicted in Fig. S6(a), found at 0.08 eV above the Fermi energy along the X–L–W high-symmetry path. Here, we discuss the principal factor contributing to the relatively modest α_{xy} observed in the stoichiometric compound. The finite BC in the stoichiometric compound, illustrated by the green curve in Fig. S6(b), is only found along the L–W high-symmetry path at 0.17 eV above ϵ_{F}. As a result, a relatively small $\partial\sigma_{xy}(\epsilon)/\partial\epsilon$ emerges within the energy range of [0.1 : 0.17] eV above the Fermi energy. This gives rise to a local minimum of $-310.49\ \mathrm{S\,cm^{-1}}$ [refer to the asterisk in Fig. S6(c)]. and consequently leads to a smaller local maximum α_{xy} of $4.24\ \mathrm{A\,m^{-1}K^{-1}}$, located at 0.13 eV above ϵ_{F}. [indicated by the asterisk in Fig. S6(d)].

Furthermore, an additional local minimum of $-353.61\ \mathrm{S\,cm^{-1}}$ at 0.3 eV above ϵ_{F} for the stoichiometric compound predominantly originates from substantial BC along the X–L high-symmetry path, as indicated by the red curve in Fig. S6(b). In essence, the reason for the observed smaller

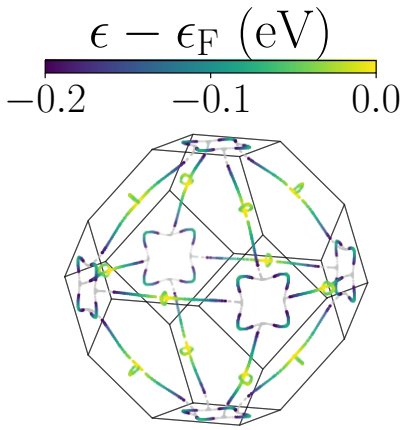

Figure S5. Nodal line network of $Fe_2Mn_{0.7}Fe_{0.3}P$ formed by two majority spin bands (see main text) that generate large σ_{xy}.

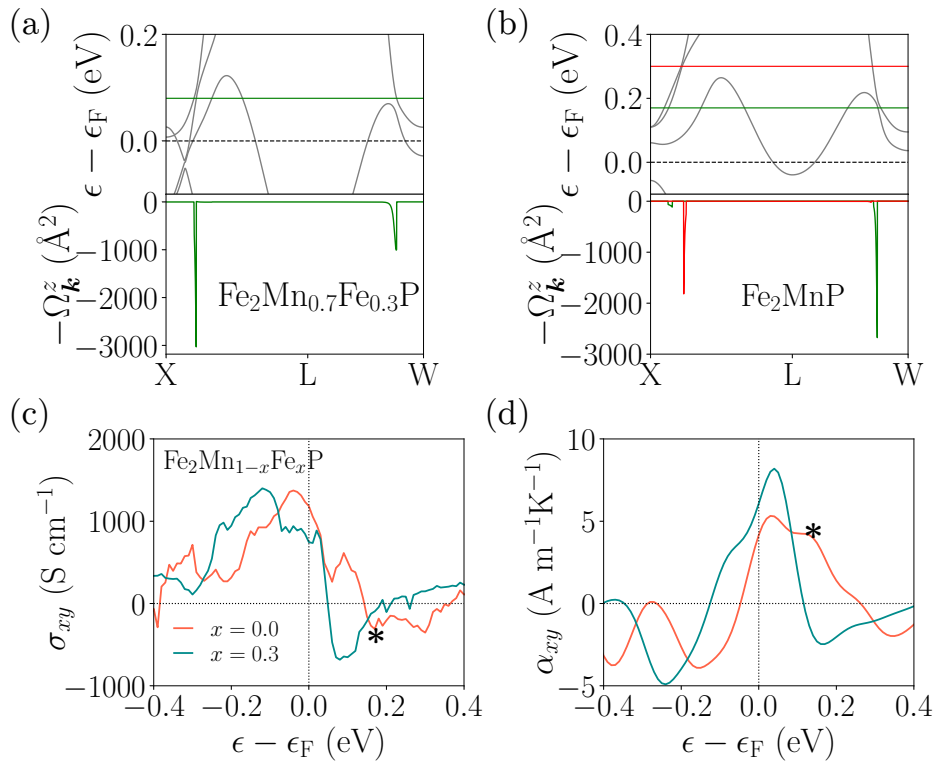

Figure S6. (a) Berry curvature of $Fe_2Mn_{0.7}Fe_{0.3}P$ (a) and Fe_2MnP (b) along the high-symmetry path. The Berry curvature for $Fe_2Mn_{0.7}Fe_{0.3}P$ is evaluated at 0.08 eV above the Fermi energy, while for Fe_2MnP it is evaluated at 0.17 (red) and 0.3 eV (blue) above the Fermi energy, respectively. Energy-dependent σ_{xy} (c) and α_{xy} (d) of $Fe_2Mn_{1-x}Fe_xP$ with $x = 0$, and 0.3, respectively.

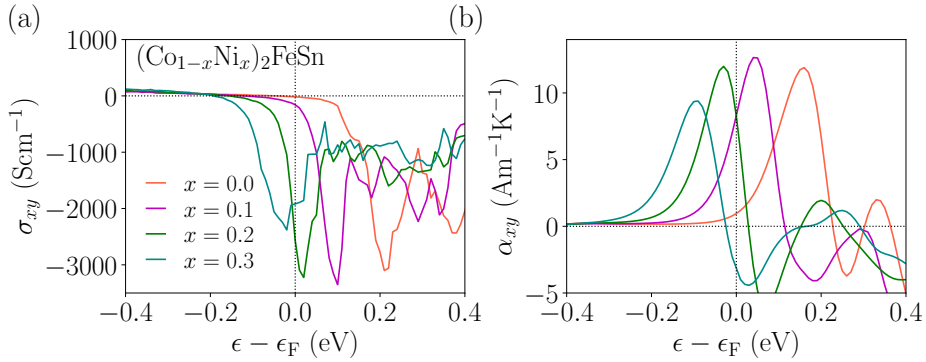

Figure S7. Energy-dependent σ_{xy} (a) and α_{xy} (b) of $(Co_{1-x}Ni_x)_2FeSn$ with $x = 0$, 0.1, 0.2, and 0.3, respectively.

local maximum α_{xy} value observed at 0.13 eV above ϵ_F in Fe_2MnP can be attributed to the divergence of anti-crossing points into two distinct energy levels. This divergence hinders the simultaneous generation of significant BC. In contrast, the simultaneous and substantial BC observed

in Fig. S6(a) lead to a noteworthy $\alpha_{xy}^{\max}$ of 8.12 $\mathrm{A\,m^{-1}K^{-1}}$ at 0.04 eV above ϵ_{F}. Additionally, the $\alpha_{xy}^{\max}$ of 5.32 $\mathrm{A\,m^{-1}K^{-1}}$ was observed at 0.03 eV above the Fermi energy, which is attributed to the slope found around the Fermi energy in Fe_2MnP.

F. Optimum anomalous transport properties through chemical substitution

Table S1. Co-based doped candidates with promising σ_{xy} at the Fermi energy. Contents in the table are the space group (SG), the calculated magtic moment m per formula unit, the σ_{xy} and α_{xy} at the Fermi energy, and the maximum value $\sigma_{xy}^{\max}$ and $\alpha_{xy}^{\max}$ obtained in an energy window 0.3 eV around the Fermi level. $\Delta\epsilon$ denotes the energy difference of the maximum values with respect to the Fermi energy.

Candidates	SG	m (μ_{B}/f.u.)	σ_{xy} ($\mathrm{S\,cm^{-1}}$)	α_{xy} ($\mathrm{A\,m^{-1}K^{-1}}$)	$\sigma_{xy}^{\max}$ [$\Delta\epsilon$] ($\mathrm{S\,cm^{-1}}$) [(eV)]	$\alpha_{xy}^{\max}$ [$\Delta\epsilon$] ($\mathrm{A\,m^{-1}K^{-1}}$) [(eV)]
$(Co_{0.8}Ni_{0.2})_2FeSn$	225	5.33	−2567.78	8.27	−3224.09 (0.02)	11.99 (−0.03)
$(Co_{0.8}Ni_{0.2})_2FeGe$	225	5.31	−1867.45	8.20	−3152.20 (0.02)	10.90 (−0.03)
$Co_2Mn_{0.9}Fe_{0.1}Ga$	225	4.20	1701.59	2.43	1701.59 (0.00)	5.15 (0.04)
$(Co_{0.7}Ni_{0.3})_2FeSi$	225	4.83	−1418.63	2.50	−2036.72 (0.19)	7.93 (−0.06)
$Co_2MnAl_{0.9}Si_{0.1}$	225	4.08	1271.53	0.24	1618.76 (−0.01)	3.69 (0.09)
$Co_2Mn_{0.9}Cr_{0.1}In$	225	4.53	1132.95	3.60	1546.55 (−0.28)	4.09 (−0.27)
$(Co_{0.7}Ni_{0.3})_2MnP$	225	5.48	−1130.86	4.02	−1328.90 (0.01)	8.44 (−0.05)
$(Co_{0.9}Fe_{0.1})_2CrGa$	225	2.82	1069.31	1.86	1246.06 (−0.01)	−5.01 (−0.28)
$(Co_{0.8}Fe_{0.2})_2CrAl$	225	2.57	1018.37	0.75	1777.19 (−0.08)	−4.21 (−0.24)
$(Co_{0.7}Ni_{0.3})_2MnSb$	225	5.50	−938.50	−0.05	−1260.77 (−0.02)	5.80 (−0.09)
Co_3Ga	225	4.27	747.47	2.04	892.29 (−0.02)	3.36 (0.05)
Co_3Al	225	4.21	714.23	1.52	1001.91 (0.27)	−3.34 (0.23)
Co_3In	225	4.42	633.37	1.47	800.33 (0.26)	3.03 (0.29)
$(Co_{0.8}Fe_{0.2})_3Ge$	225	4.63	473.19	1.38	658.98 (−0.08)	−3.45 (−0.18)
$(Co_{0.8}Fe_{0.2})_3Sn$	225	4.79	470.19	0.84	570.95 (0.30)	4.82 (0.30)
$(Co_{0.8}Fe_{0.2})_2NiAl$	216	3.71	456.14	0.82	1151.49 (0.22)	−4.30 (0.17)

Table S2. Fe-based doped candidates with promising σ_{xy} at the Fermi energy. Contents in the table are the space group (SG), the calculated magtic moment m per formula unit, the σ_{xy} and α_{xy} at the Fermi energy, and the maximum value $\sigma_{xy}^{\max}$ and $\alpha_{xy}^{\max}$ obtained in an energy window 0.3 eV around the Fermi level. $\Delta\epsilon$ denotes the energy difference of the maximum values with respect to the Fermi energy.

Candidates	SG	m (μ_B/f.u.)	σ_{xy} (S cm^{-1})	α_{xy} (A m^{-1}K^{-1})	$\sigma_{xy}^{\max}$ [$\Delta\epsilon$] (S cm^{-1}) [(eV)]	$\alpha_{xy}^{\max}$ [$\Delta\epsilon$] (A m^{-1}K^{-1}) [(eV)]
$(Fe_{0.8}Mn_{0.2})_2MnSn$	225	6.50	1598.79	0.76	1623.15 (−0.01)	4.04 (0.06)
$(Fe_{0.9}Mn_{0.1})_2CoIn$	225	7.08	1583.29	2.47	1646.07 (−0.01)	7.27 (0.07)
$Fe_2ScIn_{0.8}Sn_{0.2}$	225	3.98	1473.78	−4.17	1769.44 (0.13)	5.63 (0.16)
$(Fe_{0.8}Mn_{0.2})_3Sn$	225	7.15	1472.18	3.30	1787.16 (−0.03)	5.01 (0.04)
$Fe_2MnAs_{0.8}Ge_{0.2}$	225	3.78	1431.72	−0.71	1431.72 (0.00)	5.45 (0.08)
$Fe_2Mn_{0.7}Cr_{0.3}Sb$	225	3.68	1387.34	−0.14	1398.77 (0.01)	4.88 (0.07)
$Fe_2MnP_{0.9}Si_{0.1}$	225	3.87	1379.60	0.99	1389.77 (−0.01)	5.27 (0.07)
$Fe_2Co_{0.9}Ni_{0.1}Si$	225	4.86	1042.26	−1.16	1125.41 (0.03)	−3.87 (−0.07)
$(Fe_{0.7}Mn_{0.3})_2CoGa$	225	6.91	1035.39	1.84	1143.59 (−0.01)	5.15 (0.08)
$(Fe_{0.8}Mn_{0.2})_3Al$	225	6.68	997.30	−0.15	1156.80 (−0.27)	4.15 (−0.30)
$Fe_2Cr_{0.8}Mn_{0.2}Sn$	225	4.69	928.93	1.14	1654.31 (−0.19)	−6.19 (−0.24)
$Fe_2Co_{0.9}Fe_{0.1}In$	216	6.28	772.06	1.57	1493.68 (−0.24)	4.77 (−0.20)
$(Fe_{0.7}Co_{0.3})_2MnSi$	225	3.57	701.82	−5.05	1634.78 (−0.24)	7.12 (0.21)
$Fe_2Co_{0.7}Fe_{0.3}Ga$	216	5.83	618.72	1.55	740.52 (−0.22)	2.80 (−0.29)
$(Fe_{0.7}Mn_{0.3})_2NiIn$	216	5.66	576.99	1.53	1171.76 (−0.03)	1.98 (0.03)
$(Fe_{0.7}Co_{0.3})_3As$	225	5.97	560.68	2.79	704.92 (−0.01)	3.32 (0.02)
$Fe_2VSi_{0.7}P_{0.3}$	225	1.11	550.52	1.57	713.11 (−0.04)	2.63 (0.04)
$(Fe_{0.7}Co_{0.3})_2CrGa$	225	1.60	493.52	−2.94	1536.44 (0.08)	−2.94 (0.00)
$(Fe_{0.8}Co_{0.2})_2CrAl$	225	1.39	413.74	−2.65	1730.62 (0.11)	−4.02 (0.06)
$(Fe_{0.8}Co_{0.2})_2ScAl$	225	1.53	−397.96	−1.97	−691.30 (−0.13)	4.67 (−0.24)
$(Fe_{0.8}Co_{0.2})_2CoP$	216	5.74	391.97	−0.86	−623.42 (0.29)	4.45 (0.12)
$(Fe_{0.8}Mn_{0.2})_3Si$	225	5.32	356.54	3.28	1524.39 (−0.11)	5.77 (−0.06)
$(Fe_{0.7}Co_{0.3})_2ScGa$	225	1.33	297.87	−1.09	−571.70 (−0.25)	6.64 (−0.30)

Table S3. Mn-based doped candidates with promising σ_{xy} at the Fermi energy. Contents in the table are the space group (SG), the calculated magtic moment m per formula unit, the σ_{xy} and α_{xy} at the Fermi energy, and the maximum value $\sigma_{xy}^{\max}$ and $\alpha_{xy}^{\max}$ obtained in an energy window 0.3 eV around the Fermi level. $\Delta\epsilon$ denotes the energy difference of the maximum values with respect to the Fermi energy.

Candidates	SG	m (μ_B/f.u.)	σ_{xy} (S cm^{-1})	α_{xy} (A m^{-1}K^{-1})	$\sigma_{xy}^{\max}$ [$\Delta\epsilon$] (S cm^{-1}) [(eV)]	$\alpha_{xy}^{\max}$ [$\Delta\epsilon$] (A m^{-1}K^{-1}) [(eV)]
$Mn_2Ti_{0.9}V_{0.1}Ga$	225	2.90	1448.19	1.20	1448.19 (0.00)	3.99 (0.04)
$Mn_2Fe_{0.8}Mn_{0.2}Ga$	225	7.20	1396.36	−0.60	1586.36 (−0.02)	−3.94 (−0.05)
$Mn_2CoGe_{0.9}As_{0.1}$	225	7.64	1365.31	−0.47	1369.37 (0.01)	3.99 (0.06)
$(Mn_{0.8}Cr_{0.2})_2ScGe$	225	3.38	1161.17	0.10	1562.43 (−0.26)	−3.81 (−0.06)
$Mn_2Ti_{0.9}V_{0.1}Al$	225	2.90	1044.91	2.37	1544.45 (−0.01)	4.40 (0.03)
$(Mn_{0.7}Fe_{0.3})_2NiAl$	225	6.79	989.08	−2.21	1463.94 (0.04)	−4.04 (−0.06)
$(Mn_{0.7}Fe_{0.3})_2ScAl$	225	3.87	946.70	−4.16	1304.23 (0.07)	5.81 (0.18)
$(Mn_{0.7}Cr_{0.3})_2ScIn$	225	6.46	813.71	1.41	1104.70 (0.06)	−3.25 (−0.12)
$Mn_2Ti_{0.8}Sc_{0.2}In$	225	3.46	785.57	−1.22	966.26 (0.08)	−1.88 (−0.05)
$(Mn_{0.7}Cr_{0.3})_2ScSi$	225	3.58	692.26	−3.34	1242.33 (0.03)	−3.87 (−0.02)
$(Mn_{0.8}Cr_{0.2})_3Si$	225	0.38	−626.83	−1.38	−885.94 (−0.05)	−3.07 (0.07)
$Mn_2Ti_{0.8}Sc_{0.2}Ge$	225	2.18	385.65	0.93	813.23 (−0.30)	3.49 (−0.25)
$Mn_2Ni_{0.7}Co_{0.3}In$	225	8.22	−323.33	1.59	−357.25 (0.02)	2.33 (−0.03)

Table S4. Rh-based doped candidates with promising σ_{xy} at the Fermi energy. Contents in the table are the space group (SG), the calculated magtic moment m per formula unit, the σ_{xy} and α_{xy} at the Fermi energy, and the maximum value $\sigma_{xy}^{\max}$ and $\alpha_{xy}^{\max}$ obtained in an energy window 0.3 eV around the Fermi level. $\Delta\epsilon$ denotes the energy difference of the maximum values with respect to the Fermi energy.

Candidates	SG	m (μ_B/f.u.)	σ_{xy} (S cm^{-1})	α_{xy} (A m^{-1}K^{-1})	$\sigma_{xy}^{\max}$ [$\Delta\epsilon$] (S cm^{-1}) [(eV)]	$\alpha_{xy}^{\max}$ [$\Delta\epsilon$] (A m^{-1}K^{-1}) [(eV)]
$(Rh_{0.8}Ru_{0.2})_2MnIn$	225	3.95	1950.49	−2.14	1950.49 (0.00)	−6.67 (−0.05)
$(Rh_{0.9}Ru_{0.1})_2MnGa$	225	3.94	1894.95	−3.98	2148.66 (0.04)	−7.09 (−0.07)
Rh_2MnAl	225	4.11	1742.50	2.47	2027.10 (−0.04)	5.97 (0.09)
$Rh_2Cr_{0.9}Mn_{0.1}In$	225	3.27	1344.07	0.95	1529.13 (−0.12)	−5.51 (−0.17)
$(Rh_{0.9}Ru_{0.1})_2CrGa$	225	2.83	1316.51	−0.89	1316.51 (0.00)	−3.89 (−0.06)
Rh_2CrAl	225	3.01	1285.60	1.63	1794.87 (−0.03)	−5.15 (−0.29)
$Rh_2NiSn_{0.8}Sb_{0.2}$	225	0.99	−1104.01	6.15	−1722.29 (0.11)	7.91 (−0.06)
$Rh_2NiSi_{0.7}P_{0.3}$	225	0.92	−770.92	8.48	−1595.03 (0.06)	8.79 (−0.02)
$Rh_2FeAl_{0.8}Si_{0.2}$	225	4.19	764.20	0.37	863.80 (−0.01)	4.83 (0.17)
$(Rh_{0.7}Ru_{0.3})_2CoIn$	225	3.50	670.14	3.62	−1060.04 (0.11)	6.13 (0.05)
$(Rh_{0.7}Ru_{0.3})_2FeGe$	225	4.20	623.32	3.01	−996.44 (0.02)	8.67 (0.29)
$Rh_2Fe_{0.8}Co_{0.2}In$	225	4.06	−595.57	5.10	−1252.68 (0.05)	5.12 (0.01)
$(Rh_{0.9}Ru_{0.1})_2FeGa$	225	4.47	511.23	−1.64	511.23 (0.00)	4.60 (0.28)
$(Rh_{0.7}Ru_{0.3})_2CoGa$	225	3.39	505.69	1.91	1074.60 (0.03)	5.27 (0.06)
$Rh_2CoAl_{0.7}Si_{0.3}$	225	2.90	435.46	−1.62	506.76 (−0.29)	3.62 (0.23)
$(Rh_{0.9}Ru_{0.1})_2NiGa$	225	2.01	420.61	0.81	953.41 (−0.30)	4.59 (0.29)
$(Rh_{0.9}Ru_{0.1})_2NiAl$	225	1.98	363.69	1.25	1085.13 (−0.29)	4.32 (−0.27)

Table S5. Ru-based doped candidates with promising σ_{xy} at the Fermi energy. Contents in the table are the space group (SG), the calculated magtic moment m per formula unit, the σ_{xy} and α_{xy} at the Fermi energy, and the maximum value $\sigma_{xy}^{\max}$ and $\alpha_{xy}^{\max}$ obtained in an energy window 0.3 eV around the Fermi level. $\Delta\epsilon$ denotes the energy difference of the maximum values with respect to the Fermi energy.

Candidates	SG	m (μ_B/f.u.)	σ_{xy} (S cm^{-1})	α_{xy} (A m^{-1}K^{-1})	$\sigma_{xy}^{\max}$ [$\Delta\epsilon$] (S cm^{-1}) [(eV)]	$\alpha_{xy}^{\max}$ [$\Delta\epsilon$] (A m^{-1}K^{-1}) [(eV)]
$(Ru_{0.8}Rh_{0.2})_2FeP$	225	4.21	1436.35	−1.36	1436.35 (0.00)	4.41 (0.11)
$(Ru_{0.8}Rh_{0.2})_2CoAl$	225	2.91	1426.00	1.48	2219.34 (−0.07)	7.33 (0.09)
$Ru_2Co_{0.7}Fe_{0.3}Ge$	225	3.15	1370.43	2.54	1370.43 (0.00)	−6.49 (−0.18)
$(Ru_{0.7}Rh_{0.3})_2FeSb$	225	4.36	1146.57	−1.02	1241.76 (0.08)	6.54 (0.15)
$Ru_2Mn_{0.9}Cr_{0.1}Sb$	225	3.93	1140.69	−1.12	1161.79 (0.01)	−4.66 (−0.07)
$(Ru_{0.7}Rh_{0.3})_2CrSb$	225	3.61	1133.04	−3.74	2032.25 (−0.07)	4.76 (0.26)
$Ru_2Mn_{0.9}Fe_{0.1}P$	225	4.04	1086.88	0.47	1086.88 (0.00)	−4.59 (−0.11)
$(Ru_{0.9}Rh_{0.1})_2MnAs$	225	4.13	1069.22	3.04	1100.74 (−0.04)	−5.08 (−0.13)
$(Ru_{0.8}Rh_{0.2})_2FeAs$	225	4.29	1044.04	−2.77	1381.84 (0.07)	3.99 (0.12)
Ru_2FeSi	225	3.93	1014.70	1.33	1014.70 (0.00)	3.43 (0.06)
$Ru_2Co_{0.7}Ni_{0.3}P$	225	1.84	989.33	1.16	1026.25 (−0.03)	−4.83 (−0.13)
$Ru_2Fe_{0.9}Mn_{0.1}Ge$	225	3.94	985.44	0.84	985.44 (0.00)	−3.87 (−0.12)
$Ru_2Fe_{0.7}Mn_{0.3}Sn$	225	3.80	889.24	−1.00	946.16 (0.01)	−3.73 (−0.07)
$(Ru_{0.7}Rh_{0.3})_2FeGa$	225	3.72	884.07	−2.44	1099.03 (0.05)	3.64 (0.11)
$(Ru_{0.7}Rh_{0.3})_2FeAl$	225	3.67	859.74	−2.34	1184.26 (0.07)	4.13 (0.14)
$(Ru_{0.8}Rh_{0.2})_2CoSi$	225	2.66	814.11	2.68	1070.31 (−0.02)	3.84 (0.04)
$(Ru_{0.7}Rh_{0.3})_2MnSn$	225	3.70	758.11	−4.56	1286.89 (0.07)	−4.61 (−0.01)
$Ru_2CrSn_{0.7}In_{0.3}$	225	1.87	−666.38	0.45	−666.38 (0.00)	2.93 (−0.05)
$(Ru_{0.8}Rh_{0.2})_2CrP$	225	3.36	457.30	−1.55	1306.74 (0.11)	3.90 (0.29)
$(Ru_{0.7}Rh_{0.3})_2MnGe$	225	3.64	430.01	−3.63	1322.52 (0.12)	−3.80 (0.02)
$(Ru_{0.9}Rh_{0.1})_2CrAs$	225	3.12	408.33	−0.40	1313.59 (0.18)	−5.18 (0.13)
$(Ru_{0.7}Rh_{0.3})_2VSi$	225	1.54	378.21	−0.92	1123.37 (0.21)	−2.02 (0.06)

Table S6. Cr-based doped candidates with promising σ_{xy} at the Fermi energy. Contents in the table are the space group (SG), the calculated magtic moment m per formula unit, the σ_{xy} and α_{xy} at the Fermi energy, and the maximum value $\sigma_{xy}^{\max}$ and $\alpha_{xy}^{\max}$ obtained in an energy window 0.3 eV around the Fermi level. $\Delta\epsilon$ denotes the energy difference of the maximum values with respect to the Fermi energy.

Candidates	SG	m (μ_B/f.u.)	σ_{xy} (S cm^{-1})	α_{xy} (A m^{-1}K^{-1})	$\sigma_{xy}^{\max}$ [$\Delta\epsilon$] (S cm^{-1}) [(eV)]	$\alpha_{xy}^{\max}$ [$\Delta\epsilon$] (A m^{-1}K^{-1}) [(eV)]
$Cr_2Ti_{0.7}Sc_{0.3}As$	225	3.26	951.99	0.15	951.99 (0.00)	−2.18 (−0.05)
$(Cr_{0.7}Mn_{0.3})_2TiSb$	225	2.40	853.77	−0.23	853.77 (0.00)	2.81 (−0.14)
$(Cr_{0.7}V_{0.3})_2ScSi$	225	5.17	613.27	−1.22	613.27 (0.00)	−2.17 (−0.06)
$(Cr_{0.8}Mn_{0.2})_2ScP$	225	3.60	559.48	−1.88	1297.23 (0.03)	2.75 (0.08)
$Cr_2MnGe_{0.8}Ga_{0.2}$	225	4.80	544.09	−0.02	544.09 (0.00)	1.77 (0.26)
$Cr_2Fe_{0.7}Mn_{0.3}P$	216	0.70	−504.21	−1.75	−508.96 (0.01)	−2.93 (0.04)
$Cr_2Ti_{0.7}Sc_{0.3}Si$	225	4.01	400.80	−0.66	−979.00 (−0.27)	−2.20 (−0.05)
$(Cr_{0.8}V_{0.2})_2TiGe$	225	3.51	257.39	0.46	−518.83 (−0.18)	3.05 (−0.24)

Table S7. Ni-based doped candidates with promising σ_{xy} at the Fermi energy. Contents in the table are the space group (SG), the calculated magtic moment m per formula unit, the σ_{xy} and α_{xy} at the Fermi energy, and the maximum value $\sigma_{xy}^{\max}$ and $\alpha_{xy}^{\max}$ obtained in an energy window 0.3 eV around the Fermi level. $\Delta\epsilon$ denotes the energy difference of the maximum values with respect to the Fermi energy.

Candidates	SG	m (μ_B/f.u.)	σ_{xy} (S cm^{-1})	α_{xy} (A m^{-1}K^{-1})	$\sigma_{xy}^{\max}$ [$\Delta\epsilon$] (S cm^{-1}) [(eV)]	$\alpha_{xy}^{\max}$ [$\Delta\epsilon$] (A m^{-1}K^{-1}) [(eV)]
$(Ni_{0.8}Co_{0.2})_2MnIn$	225	4.80	−456.14	−0.85	−774.35 (−0.04)	1.63 (−0.10)
$(Ni_{0.8}Co_{0.2})_2FeSb$	225	3.47	−396.06	0.34	−508.19 (0.04)	1.95 (0.29)
$(Ni_{0.9}Co_{0.1})_2MnAl$	225	4.43	−318.29	0.53	−398.26 (−0.02)	2.40 (−0.07)

Table S8. V-based doped candidates with promising σ_{xy} at the Fermi energy. Contents in the table are the space group (SG), the calculated magtic moment m per formula unit, the σ_{xy} and α_{xy} at the Fermi energy, and the maximum value $\sigma_{xy}^{\max}$ and $\alpha_{xy}^{\max}$ obtained in an energy window 0.3 eV around the Fermi level. $\Delta\epsilon$ denotes the energy difference of the maximum values with respect to the Fermi energy.

Candidates	SG	m (μ_B/f.u.)	σ_{xy} (S cm^{-1})	α_{xy} (A m^{-1}K^{-1})	$\sigma_{xy}^{\max}$ [$\Delta\epsilon$] (S cm^{-1}) [(eV)]	$\alpha_{xy}^{\max}$ [$\Delta\epsilon$] (A m^{-1}K^{-1}) [(eV)]
$V_2Cr_{0.7}V_{0.3}Al$	225	0.54	352.33	−1.08	−1090.72 (−0.17)	−5.68 (−0.12)
$(V_{0.7}Cr_{0.3})_2TiSb$	225	3.12	234.24	−0.40	1255.83 (0.18)	2.22 (0.22)

Table S9. Co-based doped candidates with promising α_{xy} at the Fermi energy. Contents in the table are the space group (SG), the calculated magtic moment m per formula unit, the σ_{xy} and α_{xy} at the Fermi energy, and the maximum value $\sigma_{xy}^{\max}$ and $\alpha_{xy}^{\max}$ obtained in an energy window 0.3 eV around the Fermi level. $\Delta\epsilon$ denotes the energy difference of the maximum values with respect to the Fermi energy.

Candidates	SG	m (μ_B/f.u.)	σ_{xy} (Scm^{-1})	α_{xy} (Am^{-1}K^{-1})	$\sigma_{xy}^{\max}$ [$\Delta\epsilon$] (Scm^{-1}) [(eV)]	$\alpha_{xy}^{\max}$ [$\Delta\epsilon$] (Am^{-1}K^{-1}) [(eV)]
$(Co_{0.7}Ni_{0.3})_3Sn$	225	3.15	−30.66	8.56	−2614.20 (0.06)	11.48 (0.03)
$(Co_{0.9}Ni_{0.1})_2FeSn$	225	5.59	−158.04	8.31	−3351.26 (0.10)	12.65 (0.04)
$(Co_{0.8}Ni_{0.2})_2FeGe$	225	5.31	−1867.45	8.20	−3152.20 (0.02)	10.90 (−0.03)
$(Co_{0.8}Ni_{0.2})_2MnP$	225	5.84	86.84	7.36	−1548.89 (0.12)	8.41 (0.03)
$(Co_{0.7}Ni_{0.3})_3Ge$	225	3.03	156.11	6.23	−1477.30 (0.18)	7.43 (0.03)
$(Co_{0.8}Ni_{0.2})_2FeSi$	225	5.12	−605.89	5.80	−1944.35 (0.28)	6.55 (−0.02)
$(Co_{0.8}Ni_{0.2})_2MnSb$	225	5.82	−546.77	5.41	−1217.02 (0.04)	5.43 (−0.01)
$Co_2MnGa_{0.8}Ge_{0.2}$	225	4.24	831.12	4.66	1368.59 (−0.03)	4.68 (0.01)
$Co_2MnAl_{0.8}Si_{0.2}$	225	4.17	950.80	4.20	1454.80 (−0.07)	4.41 (0.02)
Co_2MnIn	225	4.76	447.94	3.87	1924.80 (−0.24)	5.03 (−0.06)
$(Co_{0.9}Ni_{0.1})_3Ga$	225	3.98	435.88	3.59	961.37 (−0.09)	3.67 (0.02)
$(Co_{0.9}Ni_{0.1})_3Al$	225	3.93	368.36	3.57	1562.10 (0.19)	−4.18 (0.15)
$(Co_{0.7}Fe_{0.3})_2CrGa$	225	2.41	701.27	3.36	2043.27 (−0.04)	−8.17 (−0.14)
$(Co_{0.9}Fe_{0.1})_2CrAl$	225	2.77	629.76	3.02	1168.69 (−0.01)	3.55 (0.02)
$(Co_{0.9}Ni_{0.1})_3In$	225	4.09	308.08	2.73	724.61 (−0.08)	6.27 (0.29)
$(Co_{0.9}Fe_{0.1})_2NiAl$	216	3.46	215.79	1.99	1234.34 (0.16)	−3.75 (0.12)

Table S10. Fe-based doped candidates with promising α_{xy} at the Fermi energy. Contents in the table are the space group (SG), the calculated magtic moment m per formula unit, the σ_{xy} and α_{xy} at the Fermi energy, and the maximum value $\sigma_{xy}^{\max}$ and $\alpha_{xy}^{\max}$ obtained in an energy window 0.3 eV around the Fermi level. $\Delta\epsilon$ denotes the energy difference of the maximum values with respect to the Fermi energy.

Candidates	SG	m (μ_B/f.u.)	σ_{xy} (Scm^{-1})	α_{xy} (Am^{-1}K^{-1})	$\sigma_{xy}^{\max}$ [$\Delta\epsilon$] (Scm^{-1}) [(eV)]	$\alpha_{xy}^{\max}$ [$\Delta\epsilon$] (Am^{-1}K^{-1}) [(eV)]
$Fe_2CoIn_{0.9}Sn_{0.1}$	225	6.82	802.75	6.81	1815.55 (0.27)	6.81 (0.00)
$Fe_2Mn_{0.7}Fe_{0.3}P$	225	4.30	745.39	6.08	1400.34 (−0.12)	8.19 (0.04)
$(Fe_{0.8}Mn_{0.2})_2MnAs$	225	3.57	1207.02	−5.99	1408.86 (0.06)	7.62 (0.23)
$(Fe_{0.7}Co_{0.3})_2MnSi$	225	3.57	701.82	−5.05	1634.78 (−0.24)	7.12 (0.21)
$(Fe_{0.7}Co_{0.3})_2CrAl$	225	1.59	413.14	−4.90	1695.66 (0.08)	−5.40 (0.03)
$Fe_2Mn_{0.9}Cr_{0.1}Sn$	225	5.94	929.58	4.70	2006.10 (−0.09)	5.16 (−0.02)
$(Fe_{0.9}Mn_{0.1})_3Sn$	225	6.95	715.93	4.64	1849.10 (−0.09)	5.05 (−0.02)
$Fe_2Co_{0.8}Ni_{0.2}Ga$	225	6.18	212.84	−4.59	1700.37 (0.23)	6.00 (−0.11)
$(Fe_{0.8}Mn_{0.2})_2CoSi$	225	5.10	330.44	−4.59	1162.46 (0.10)	−4.68 (0.01)
$Fe_2ScIn_{0.9}Sn_{0.1}$	225	4.01	654.43	−4.58	1437.36 (0.12)	4.85 (0.17)
$(Fe_{0.7}Mn_{0.3})_3Al$	225	6.83	480.17	−3.70	2170.11 (−0.29)	6.16 (−0.25)
$(Fe_{0.7}Co_{0.3})_2CoP$	216	5.60	273.62	3.65	−848.66 (0.28)	4.14 (0.02)
$(Fe_{0.7}Co_{0.3})_2ScAl$	225	1.30	−78.92	−3.61	−893.14 (−0.19)	5.61 (−0.29)
$(Fe_{0.8}Co_{0.2})_2CrGa$	225	0.73	316.34	−3.53	868.19 (0.04)	4.18 (0.18)
$(Fe_{0.8}Mn_{0.2})_3Si$	225	5.32	356.54	3.28	1524.39 (−0.11)	5.77 (−0.06)
$Fe_2Cr_{0.7}Mn_{0.3}Sn$	225	4.85	910.52	3.16	2103.23 (−0.22)	−8.33 (−0.25)
$(Fe_{0.7}Mn_{0.3})_2MnSb$	225	5.42	473.06	2.94	2309.91 (−0.22)	6.54 (−0.14)
$Fe_2CoIn_{0.9}Sn_{0.1}$	216	6.14	301.25	2.89	1122.48 (−0.29)	4.20 (−0.27)
$(Fe_{0.7}Co_{0.3})_3As$	225	5.97	560.68	2.79	704.92 (−0.01)	3.32 (0.02)
$(Fe_{0.7}Mn_{0.3})_2ScGa$	225	2.65	287.33	2.54	1473.84 (−0.15)	4.70 (−0.09)
$Fe_2Ni_{0.7}Co_{0.3}In$	216	5.53	186.71	2.44	1006.76 (−0.10)	3.02 (−0.03)
$Fe_2Co_{0.8}Fe_{0.2}Ga$	216	5.75	425.83	2.20	753.58 (−0.29)	2.20 (0.00)
$(Fe_{0.7}Co_{0.3})_2VSi$	225	1.47	−5.26	1.99	621.25 (−0.08)	2.50 (−0.03)

Table S11. Mn-based doped candidates with promising α_{xy} at the Fermi energy. Contents in the table are the space group (SG), the calculated magtic moment m per formula unit, the σ_{xy} and α_{xy} at the Fermi energy, and the maximum value $\sigma_{xy}^{\max}$ and $\alpha_{xy}^{\max}$ obtained in an energy window 0.3 eV around the Fermi level. $\Delta\epsilon$ denotes the energy difference of the maximum values with respect to the Fermi energy.

Candidates	SG	m (μ_B/f.u.)	σ_{xy} (Scm^{-1})	α_{xy} (Am^{-1}K^{-1})	$\sigma_{xy}^{\max}$ [$\Delta\epsilon$] (Scm^{-1}) [(eV)]	$\alpha_{xy}^{\max}$ [$\Delta\epsilon$] (Am^{-1}K^{-1}) [(eV)]
$(Mn_{0.8}Cr_{0.2})_2FeGa$	225	7.03	463.05	−4.94	2130.25 (0.08)	4.98 (0.13)
$(Mn_{0.9}Fe_{0.1})_2TiGa$	225	2.82	400.87	4.71	1431.43 (−0.06)	4.81 (−0.01)
$(Mn_{0.7}Fe_{0.3})_2CoGe$	225	7.37	508.27	4.55	1315.63 (−0.07)	4.55 (0.00)
$(Mn_{0.9}Fe_{0.1})_2TiAl$	225	2.81	121.81	4.39	1711.06 (−0.07)	4.83 (−0.02)
$(Mn_{0.7}Fe_{0.3})_2ScAl$	225	3.87	946.70	−4.16	1304.23 (0.07)	5.81 (0.18)
$(Mn_{0.7}Cr_{0.3})_2ScSi$	225	3.58	692.26	−3.34	1242.33 (0.03)	−3.87 (−0.02)
$Mn_2NiAl_{0.7}Si_{0.3}$	225	7.05	−52.13	−3.29	900.54 (0.09)	−3.64 (0.02)
$(Mn_{0.7}Cr_{0.3})_2ScGe$	225	3.58	494.56	−3.26	1142.28 (0.06)	−3.35 (−0.01)
$(Mn_{0.9}Cr_{0.1})_3Si$	225	0.68	−248.65	−2.88	−966.70 (−0.15)	−3.44 (−0.03)
$(Mn_{0.8}Cr_{0.2})_2ScIn$	225	6.36	440.14	2.86	1006.45 (−0.10)	−2.95 (−0.15)
$Mn_2Ti_{0.8}V_{0.2}In$	225	3.78	375.80	2.27	828.78 (−0.14)	2.41 (−0.02)
$Mn_2Ni_{0.7}Co_{0.3}In$	225	8.22	−323.33	1.59	−357.25 (0.02)	2.33 (−0.03)
Mn_2TiGe	225	1.98	41.97	1.52	−378.26 (0.08)	3.79 (−0.29)

Table S12. Rh-based doped candidates with promising α_{xy} at the Fermi energy. Contents in the table are the space group (SG), the calculated magtic moment m per formula unit, the σ_{xy} and α_{xy} at the Fermi energy, and the maximum value $\sigma_{xy}^{\max}$ and $\alpha_{xy}^{\max}$ obtained in an energy window 0.3 eV around the Fermi level. $\Delta\epsilon$ denotes the energy difference of the maximum values with respect to the Fermi energy.

Candidates	SG	m (μ_B/f.u.)	σ_{xy} (Scm^{-1})	α_{xy} (Am^{-1}K^{-1})	$\sigma_{xy}^{\max}$ [$\Delta\epsilon$] (Scm^{-1}) [(eV)]	$\alpha_{xy}^{\max}$ [$\Delta\epsilon$] (Am^{-1}K^{-1}) [(eV)]
$Rh_2Co_{0.7}Fe_{0.3}In$	225	3.43	394.57	8.57	−1649.50 (0.10)	9.74 (0.03)
$Rh_2NiSi_{0.7}P_{0.3}$	225	0.92	−770.92	8.48	−1595.03 (0.06)	8.79 (−0.02)
Rh_2NiSn	225	1.15	−545.48	7.56	−1728.71 (0.14)	7.56 (0.00)
$Rh_2Co_{0.7}Fe_{0.3}Ga$	225	3.44	284.36	6.96	−1844.04 (0.10)	9.35 (0.04)
$Rh_2MnGa_{0.8}Ge_{0.2}$	225	4.31	1012.05	6.47	2374.07 (−0.13)	−8.67 (−0.22)
$Rh_2Co_{0.7}Fe_{0.3}Al$	225	3.47	344.62	6.29	−1778.14 (0.11)	9.67 (0.05)
$Rh_2MnAl_{0.8}Si_{0.2}$	225	4.28	1178.80	5.95	2187.48 (−0.12)	5.95 (0.00)
$Rh_2Mn_{0.9}Cr_{0.1}In$	225	4.29	1413.77	5.87	1985.98 (−0.05)	−6.72 (−0.13)
$(Rh_{0.7}Ru_{0.3})_2CrIn$	225	2.51	123.31	−5.74	1295.38 (0.04)	−5.87 (0.01)
$Rh_2Fe_{0.8}Co_{0.2}In$	225	4.06	−595.57	5.10	−1252.68 (0.05)	5.12 (0.01)
$(Rh_{0.8}Ru_{0.2})_2CrAl$	225	2.61	775.06	−4.11	1384.58 (0.04)	−4.12 (−0.01)
$(Rh_{0.7}Ru_{0.3})_2CrGa$	225	2.43	300.99	−3.80	1446.90 (0.23)	−4.12 (0.02)
$Rh_2FeGa_{0.7}Ge_{0.3}$	225	4.08	50.33	3.30	−907.58 (0.07)	3.93 (0.29)
$(Rh_{0.7}Ru_{0.3})_2FeGe$	225	4.20	623.32	3.01	−996.44 (0.02)	8.67 (0.29)
$Rh_2Fe_{0.9}Mn_{0.1}Al$	225	4.43	262.70	−2.20	824.08 (0.09)	5.29 (0.26)
$Rh_2Ni_{0.9}Co_{0.1}Al$	225	2.02	254.27	2.11	−791.36 (0.29)	4.72 (0.28)
$Rh_2Ni_{0.9}Co_{0.1}Ga$	225	2.02	313.48	1.62	738.58 (−0.27)	6.18 (0.29)

Table S13. Ru-based doped candidates with promising α_{xy} at the Fermi energy. Contents in the table are the space group (SG), the calculated magtic moment m per formula unit, the σ_{xy} and α_{xy} at the Fermi energy, and the maximum value $\sigma_{xy}^{\max}$ and $\alpha_{xy}^{\max}$ obtained in an energy window 0.3 eV around the Fermi level. $\Delta\epsilon$ denotes the energy difference of the maximum values with respect to the Fermi energy.

Candidates	SG	m (μ_B/f.u.)	σ_{xy} (Scm^{-1})	α_{xy} (Am^{-1}K^{-1})	$\sigma_{xy}^{\max}$ [$\Delta\epsilon$] (Scm^{-1}) [(eV)]	$\alpha_{xy}^{\max}$ [$\Delta\epsilon$] (Am^{-1}K^{-1}) [(eV)]
$Ru_2CoAl_{0.8}Si_{0.2}$	225	2.40	406.58	6.22	1480.71 (0.23)	−9.82 (0.19)
$Ru_2Mn_{0.9}Cr_{0.1}P$	225	3.85	498.27	−5.41	1190.01 (0.09)	5.56 (0.17)
$Ru_2Mn_{0.9}Cr_{0.1}As$	225	3.83	579.02	−5.05	1177.03 (0.07)	−5.11 (−0.01)
$Ru_2Mn_{0.7}Cr_{0.3}Sb$	225	3.73	592.00	−4.77	1298.23 (0.07)	−4.77 (0.00)
Ru_2FeP	225	4.26	339.75	−4.68	1591.51 (0.07)	−5.27 (0.02)
$(Ru_{0.8}Rh_{0.2})_2CrSb$	225	3.41	525.47	−4.66	1542.99 (0.10)	−4.77 (0.01)
$Ru_2Co_{0.7}Fe_{0.3}P$	225	2.80	285.38	4.59	1246.46 (−0.13)	4.81 (−0.02)
$(Ru_{0.7}Rh_{0.3})_2MnSn$	225	3.70	758.11	−4.56	1286.89 (0.07)	−4.61 (−0.01)
$Ru_2CoGe_{0.9}As_{0.1}$	225	2.21	499.65	−4.16	979.90 (0.17)	−4.98 (−0.03)
$Ru_2Cr_{0.8}V_{0.2}As$	225	2.71	92.75	−3.97	1165.73 (0.27)	−4.13 (0.22)
$Ru_2Co_{0.9}Fe_{0.1}Si$	225	2.40	136.82	−3.90	942.81 (−0.29)	−4.17 (0.02)
$(Ru_{0.7}Rh_{0.3})_2MnGe$	225	3.64	430.01	−3.63	1322.52 (0.12)	−3.80 (0.02)
$Ru_2Fe_{0.9}Co_{0.1}As$	225	4.20	793.02	−3.59	1232.81 (0.04)	4.11 (0.15)
$Ru_2Fe_{0.7}Mn_{0.3}Ge$	225	3.74	619.29	−3.54	1021.12 (0.08)	−3.88 (−0.04)
$Ru_2Fe_{0.7}Mn_{0.3}Si$	225	3.71	513.30	−3.49	1122.02 (0.12)	3.74 (0.18)
$(Ru_{0.8}Rh_{0.2})_2FeGa$	225	3.53	384.30	−3.15	1090.70 (0.12)	3.48 (0.18)
$Ru_2Fe_{0.9}Mn_{0.1}Sn$	225	4.03	431.43	2.70	893.07 (−0.07)	−3.95 (−0.16)
$(Ru_{0.7}Rh_{0.3})_2FeAl$	225	3.67	859.74	−2.34	1184.26 (0.07)	4.13 (0.14)
$Ru_2Cr_{0.8}V_{0.2}P$	225	2.76	89.01	−2.26	1162.72 (0.27)	−3.38 (0.22)
$Ru_2Cr_{0.7}V_{0.3}Sn$	225	1.78	24.53	1.92	393.88 (−0.05)	1.92 (0.00)
$(Ru_{0.9}Rh_{0.1})_2FeSb$	225	4.39	241.05	−1.82	1056.85 (0.05)	2.35 (0.17)
$(Ru_{0.8}Rh_{0.2})_2VSi$	225	1.35	247.16	−1.40	1006.25 (0.26)	3.17 (0.29)

Table S14. Cr-based doped candidates with promising α_{xy} at the Fermi energy. Contents in the table are the space group (SG), the calculated magtic moment m per formula unit, the σ_{xy} and α_{xy} at the Fermi energy, and the maximum value $\sigma_{xy}^{\max}$ and $\alpha_{xy}^{\max}$ obtained in an energy window 0.3 eV around the Fermi level. $\Delta\epsilon$ denotes the energy difference of the maximum values with respect to the Fermi energy.

Candidates	SG	m (μ_B/f.u.)	σ_{xy} (Scm^{-1})	α_{xy} (Am^{-1}K^{-1})	$\sigma_{xy}^{\max}$ [$\Delta\epsilon$] (Scm^{-1}) [(eV)]	$\alpha_{xy}^{\max}$ [$\Delta\epsilon$] (Am^{-1}K^{-1}) [(eV)]
$Cr_2Fe_{0.8}Mn_{0.2}P$	216	0.79	−31.04	−3.21	654.09 (0.29)	−3.21 (0.00)
$(Cr_{0.7}Mn_{0.3})_2ScP$	225	3.39	514.02	2.54	1280.13 (−0.03)	2.81 (0.02)
$(Cr_{0.9}Mn_{0.1})_2TiAs$	225	2.81	619.69	2.42	758.96 (−0.08)	−2.77 (−0.12)
$(Cr_{0.9}V_{0.1})_2TiSb$	225	3.21	79.48	2.31	1367.10 (−0.05)	2.33 (−0.01)
$Cr_2Mn_{0.7}Fe_{0.3}Ge$	225	4.78	285.88	1.97	552.04 (−0.06)	−2.42 (0.28)
$(Cr_{0.7}V_{0.3})_2TiGe$	225	3.34	109.03	−1.75	580.18 (−0.17)	2.20 (−0.23)
$Cr_2Ti_{0.7}V_{0.3}Si$	225	3.16	175.84	−1.34	1059.06 (0.12)	2.26 (0.17)
$(Cr_{0.7}Mn_{0.3})_2ScSi$	225	4.39	257.95	1.23	709.41 (−0.01)	−2.65 (0.27)

Table S15. Ni-based doped candidates with promising α_{xy} at the Fermi energy. Contents in the table are the space group (SG), the calculated magtic moment m per formula unit, the σ_{xy} and α_{xy} at the Fermi energy, and the maximum value $\sigma_{xy}^{\max}$ and $\alpha_{xy}^{\max}$ obtained in an energy window 0.3 eV around the Fermi level. $\Delta\epsilon$ denotes the energy difference of the maximum values with respect to the Fermi energy.

Candidates	SG	m (μ_B/f.u.)	σ_{xy} (Scm^{-1})	α_{xy} (Am^{-1}K^{-1})	$\sigma_{xy}^{\max}$ [$\Delta\epsilon$] (Scm^{-1}) [(eV)]	$\alpha_{xy}^{\max}$ [$\Delta\epsilon$] (Am^{-1}K^{-1}) [(eV)]
$Ni_2FeSb_{0.8}Sn_{0.2}$	225	3.40	−210.64	−2.73	−456.81 (−0.06)	4.00 (0.29)
$(Ni_{0.7}Co_{0.3})_2MnIn$	225	5.01	−382.82	1.69	−795.55 (0.05)	2.12 (−0.27)
$Ni_2Mn_{0.7}Fe_{0.3}Al$	225	4.13	−186.71	−1.15	−530.25 (−0.22)	3.07 (−0.24)

Table S16. V-based doped candidates with promising α_{xy} at the Fermi energy. Contents in the table are the space group (SG), the calculated magtic moment m per formula unit, the σ_{xy} and α_{xy} at the Fermi energy, and the maximum value $\sigma_{xy}^{\max}$ and $\alpha_{xy}^{\max}$ obtained in an energy window 0.3 eV around the Fermi level. $\Delta\epsilon$ denotes the energy difference of the maximum values with respect to the Fermi energy.

Candidates	SG	m (μ_B/f.u.)	σ_{xy} (Scm^{-1})	α_{xy} (Am^{-1}K^{-1})	$\sigma_{xy}^{\max}$ [$\Delta\epsilon$] (Scm^{-1}) [(eV)]	$\alpha_{xy}^{\max}$ [$\Delta\epsilon$] (Am^{-1}K^{-1}) [(eV)]
$(V_{0.8}Ti_{0.2})_2TiSb$	225	0.21	−83.71	3.13	942.64 (−0.06)	−5.09 (−0.10)
$V_2CrAl_{0.8}Si_{0.2}$	225	1.17	239.69	−2.35	437.09 (0.06)	2.93 (0.16)